Spin-gap mode in the charge-ordered phase of NaV_2O_5 studied by Raman scattering under high pressures

Yoshiko Tanokura, Takayuki Morita, Shuhei Ishima, Shunsuke Ikeda, Haruhiko Kuroe, and Tomoyuki Sekine*
Department of Physics, Sophia University, 7-1 Kioi-cho, Chiyoda-ku, Tokyo 102-8554, Japan

Masahiko Isobe and Yutaka Ueda
Institute for Solid State Physics, University of Tokyo, 5-1-5 Kashiwanoha, Kashiwa-shi, Chiba 277-8581, Japan
(Received 14 April 2009; published 5 February 2010)

By means of Raman-scattering measurement under pressures at low temperatures we study the "devil's staircase"-type phase of NaV_2O_5. The spin-gap mode shows a drastic softening with increasing pressure up to 0.9 GPa in $C_{1/4}$ phase and disappears between 0.9 and 1 GPa. It appears again between 1 and 2.3 GPa in C_0 phase, indicating that this phase is also a spin-gap state. Taking the charge ordering into consideration, we discuss the spin-gap states and clarify that the spin-gap mode is created by the exchange-interaction Raman-scattering mechanism and it comes from a gap between the spin-singlet ground state and the $S_x=0$ spin-triplet excited one. This model explains that the spin gap is almost independent of the applied magnetic field and it vanishes at about 10° lower than the critical temperature in $C_{1/4}$ phase.

DOI: 10.1103/PhysRevB.81.054407 PACS number(s): 78.30.−j, 62.50.−p, 75.90.+w

I. INTRODUCTION

Since Isobe and Ueda[1] reported that the magnetic susceptibility of NaV_2O_5 rapidly decreased below $T_c=34$ K, many experimental and theoretical studies on the phase transition at T_c have been carried out. This compound contains the VO_5 pyramids, two dimensionally connected in the *ab* plane, and forms a quarter-filled ladder structure along the *b* axis. The plains stacked along the *c* axis are separated by Na ions. The VO_5 pyramids in the adjacent ladder on the same plain are pointing to opposite *c* directions each other. At room temperature, all V atoms have an averaged charge of $V^{4.5+}$. Below $T_c=34$ K, a zigzag charge order is formed[2–4] and a spin-singlet pair is created on the two adjacent rungs in a ladder, resulting in an appearance of a spin gap between the spin-singlet ground and spin-triplet excited states. The important fact is that the charge ordering is not perfect, i.e., the charge of the one side of a rung is $V^{4.5+\delta}$ and that of the other side is $V^{4.5-\delta}$, where δ is the charge disproportion parameter.[2,8] It was estimated as about 0.3 far below T_c.[4,8] The low-temperature lattice structure ($C_{1/4}$ phase) was first reported to be $2a\times 2b\times 4c$ superlattice[3,5] but later Sawa *et al.*[4] determined by a synchrotron-radiation x-ray-diffraction study that $C_{1/4}$ phase of this compound was monoclinic with a space group C_2^3-*A*112 and the superlattice structure was $(a-b)\times 2b\times 4c$. Ohwada *et al.*[6] determined the stacking pattern along the *c* axis as $AAA'A'$ by comparing the resonant x-ray scattering results with model calculations. Here, four types of possible in-plane configuration, *A*, *A'*, *B*, and *B'*, can be considered.

Inelastic neutron scattering from the spin gap was first reported using powder samples by Fujii *et al.*[5] Yosihama *et al.*[7] observed the spin gap of about 81 cm^{-1} ($\simeq$10 meV) at $\boldsymbol{q}=(3,1/2,0)$ in NaV_2O_5 single crystal and two branches with a weak dispersion along a^* direction. Grenier *et al.*[8] observed the detailed dispersion curves of two branches of magnetic excitations along the a^* and b^* axes by inelastic neutron scattering. One is at $E_g^+=66$ cm^{-1} (=8.2 meV) and the other at $E_g^-=87$ cm^{-1} (=10.8 meV) at $\boldsymbol{q}_{m1}=(0,0,0)$ and $\boldsymbol{q}_{m2}=(1/2,1/2,0)$, which are the magnetic Γ point and equivalent to each other.[9] The E_g^+ spin gap was also observed by electron-spin resonance (ESR) (Refs. 10–12) and far-infrared spectroscopy.[13,14]

Meanwhile, a peak, which grows enough below T_c and coincides approximately with the E_g^+ spin-gap energy, was observed at about 64 cm^{-1} by Raman-scattering measurements.[15–19] Moreover, Konstantinović *et al.*[20] found another peak at 86 cm^{-1}, which probably corresponds to the E_g^- magnetic excitation, by means of Raman scattering using the 647.1 nm light of Kr^+-ion laser. Gozar and Blumberg[21] studied it by Raman scattering under high magnetic fields. It splits into two peaks when magnetic fields are applied parallel to the *b* and *c* axes, strongly indicating that it is assigned as a gap mode between the spin-singlet ground state and the spin-triplet excited one. However, it neither shifts nor splits when a magnetic field is parallel to the *a* axis. On the other hand, the 64 cm^{-1} Raman peak that coincides with the E_g^+ spin-gap energy is almost independent of the magnetic field, although a shift of about 1 cm^{-1} was observed as the magnetic field was varied from 0 to 8.9 T,[17,21] which suggests that it might be spin-singlet two-magnetic-excitation bound state or a phononic excitation rather than the one-magnetic excitation. In the case of the bound state, however, it is difficult to understand why its binding is so large and equal to the spin-gap energy. Then the assignment for the 64 cm^{-1} Raman peak is still controversial.

Ohwada *et al.*[22,23] also studied the crystal structure under high pressures at low temperatures by synchrotron-radiation x-ray diffraction. They obtained a temperature-pressure (*T*-*P*) phase diagram between 0 and 2 GPa. It shows that the critical temperature T_c decreases with increasing pressure. The most characteristic feature of the phase diagram is an appearance of many complicated superlattice structures with *c*-axis modulations, i.e., "devil's staircase"-type phase. The high-pressure phase above 1 GPa has a $(a-b)\times 2b\times 1c$ superlattice structure (C_0 phase) at low temperatures. Kremer

 ©2010 The American Physical Society

et al.[24] studied the pressure dependence of the folded phonon appearing newly at 950 cm^{-1} in $C_{1/4}$ phase by Raman scattering below 1 GPa but they did not observe the spin-gap mode in the low-frequency region. To our knowledge, there is no experimental study on the spin gap under high pressures. Then we study the 64 cm^{-1} Raman mode in the devil's staircase-type phase of NaV_2O_5 by means of Raman scattering under high pressures at low temperatures.

In this paper, we report that the 64 cm^{-1} Raman mode peak strongly depends on pressure and clarify that it is one of the two spin-gap modes, i.e., the E_g^+ spin gap observed at the magnetic Γ point by inelastic neutron scattering.[8] It is activated by a mixing between the spin-singlet ground state and the $S_x=0$ spin-triplet excited one, which originates from the charge ordering. It explains that this peak is independent of applied magnetic field.

II. EXPERIMENTS

Hydrostatic pressures were applied by using a clamp-type diamond-anvil cell together with IIa-type artificial diamond crystals in order to avoid luminescence. We used 4:1 methanol-ethanol mixture as a pressure medium. Samples were cleaved along the *ab* plane and put into the gasket hole with a diameter of about 300 μm. The cell was mounted in a helium-gas-flow-type cryostat with temperature regulation better than ± 0.3 K. Pressure was measured *in situ* using the ruby-luminescence method. Raman spectra with the $c(b,b+a)\bar{c}$ and $c(a,b+a)\bar{c}$ polarization configurations were excited on the cleavage surface by using the 514.5 and 488.0 nm lines of Ar^+-ion laser. The spectra were dispersed by a Jobin-Yvon T64000 triple-grating monochromator equipped with a microscope and detected by a liquid N_2-cooled charge-coupled-device detector. The magnetic field was applied nearly parallel to the *c* axis using a split-type superconducting magnet (Oxford Instruments, Spectromag).

III. RESULTS

Figure 1 shows the pressure dependence of Raman spectrum below 330 cm^{-1} at 6 K. A Raman peak observed at 64 cm^{-1} at 0 GPa is strongly dependent on pressure. Hereafter, we call it the 64 cm^{-1} mode, whose assignment will be discussed later. Moreover, we observed three strong phonon peaks at 179, 234, and 305 cm^{-1}. The 305 cm^{-1} peak has a shoulder of a weak phonon peak at 298 cm^{-1}. Three weak peaks at 90, 105, and 132 cm^{-1} were assigned as a Raman-active phonon in the normal phase, a folded phonon, and a two-spin-gap Raman peak, respectively.[15] With increasing pressure up to 0.9 GPa the 64 cm^{-1} mode drastically softens together with a decrease in the intensity. The Rayleigh tail strongly emerges instead of the disappearance of the 64 cm^{-1} mode at 0.91 GPa, suggesting the existence of the strong fluctuations in the vicinity of the phase transition.[25,26] However, the 64 cm^{-1} mode appears again at about 28 cm^{-1} above 1.15 GPa and vanishes at 2.71 GPa. The inset of Fig. 1 shows the pressure dependence of the frequency of the 64 cm^{-1} mode. The dotted line is only guide for the eye. This result suggests that the 64 cm^{-1} mode is assigned as the

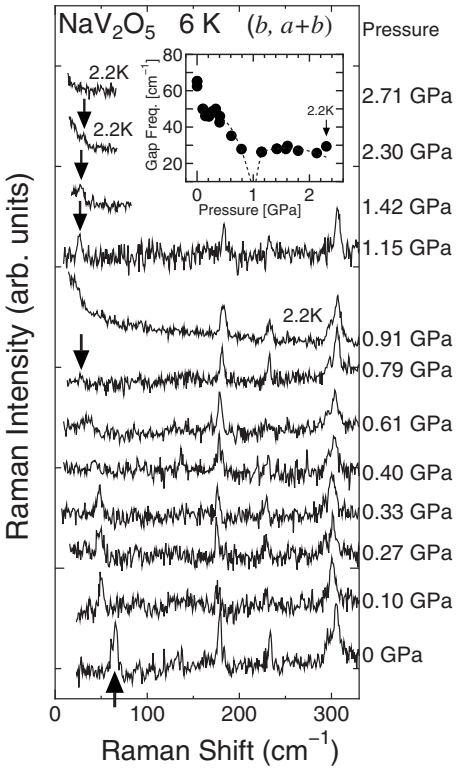

FIG. 1. Pressure dependence of Raman spectrum below 330 cm^{-1} in the $c(b,b+a)\bar{c}$ polarization configuration. The peak pointed by an arrow is the 64 cm^{-1} mode. The inset shows the frequency of the 64 cm^{-1} mode as a function of pressure. The dotted line is only guide for the eye.

spin-gap mode or a soft phonon. Grenier *et al.*[8] observed two branches of the spin-gap excitation, whose energies are E_g^+ and E_g^-, by inelastic neutron scattering. One is at $E_g^+=66.1$ cm^{-1} (=8.2 meV) and the other at $E_g^-=87.1$ cm^{-1} (=10.8 meV) at $\boldsymbol{q}_{m1}=(0,0,0)$ and $\boldsymbol{q}_{m2}=(1/2,1/2,0)$, which are the magnetic Γ points and equivalent to each other.[9] The 64 cm^{-1} mode approximately agrees with the energy of E_g^+ mode at the magnetic Γ point. It should be noted that the magnetic Γ points do not correspond to the lattice-modulation wave vector $\boldsymbol{q}_s=(1/2,1/2,1/4)$. This fact strongly suggests that the 64 cm^{-1} mode is assigned as it because the spin-gap mode at the magnetic Γ point can be observed by Raman scattering when the spin-singlet ground state is mixed with the spin-triplet excited state.[27,28] Moreover, we emphasize that the corresponding peak above 1.15 GPa is also assigned as the spin-gap mode.

On the other hand, the phonon peaks shift to higher frequency (see Fig. 2), which has been frequently observed in usual materials. Loa *et al.*[29] studied many phonons in NaV_2O_5 by Raman scattering at room temperature under high pressures up to 33 GPa and they reported a structural phase transition near 25 GPa. Our result is consistent with the result in their low-pressure region. The folded phonon at 105 cm^{-1} and the two-spin-gap Raman peak at 132 cm^{-1} rapidly disappear.

We measured the temperature dependence of the 64 cm^{-1} mode at each pressure and obtained the integrated Raman intensity normalized by the phonon peak at 179 or

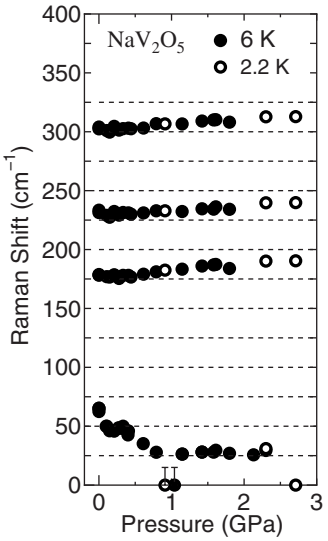

FIG. 2. Pressure dependence of the frequencies of the 64 cm^{-1} mode and the 179, 234, and 305 cm^{-1} phonon modes. The frequencies of the 64 cm^{-1} mode at 0.91 and 1.04 GPa were not precisely determined due to the strong Rayleigh tail.

305 cm^{-1}, as a function of temperature. For example, Fig. 3 shows the temperature dependence of Raman spectra from the 64 cm^{-1} mode and the 305 cm^{-1} phonon at 0.108 GPa. They were fitted by the following spectrum function:

$$I(\omega) = \frac{k^2\Gamma}{(\omega-\omega_0)^2+\Gamma^2}\{n(\omega)+1\} + \text{background}, \qquad (1)$$

where ω_0, Γ, and k are the frequency of the 64 cm^{-1} mode (the 305 cm^{-1} phonon), its damping constant, and the coupling coefficient between it and the incident light, respectively. $n(\omega)$ is the Bose factor. The fitted curves are denoted by solid lines in Fig. 3. The integrated Raman intensity of the 64 cm^{-1} mode is normalized by the 305 cm^{-1} phonon, which appears at 302 cm^{-1}, and plotted in Fig. 4 as a function of temperature. Later, we will discuss the temperature dependence of the intensity in detail. Here we fit it temporarily with a linear function, i.e., a function of $[1-(T/T_0)]^{2\beta'}$ with $\beta'=0.5$, by the least-square method, because the S/N ratio of the spectrum was worse near T_0 and we were not able to determine the parameter β'. We estimated the temperature T_0 where the normalized intensity vanished. In this case it was about 24 K. Temperature dependence of the frequency and damping constant of the 64 cm^{-1} mode at 0.108 GPa is also plotted in Fig. 4. The intensity is rapidly reduced while the frequency is almost unchanged. This result coincides with the behavior of the spin gap, which was observed by ESR (Refs. 11 and 12) and by far-infrared spectroscopy.[14] The damping constant Γ is almost independent of temperature.

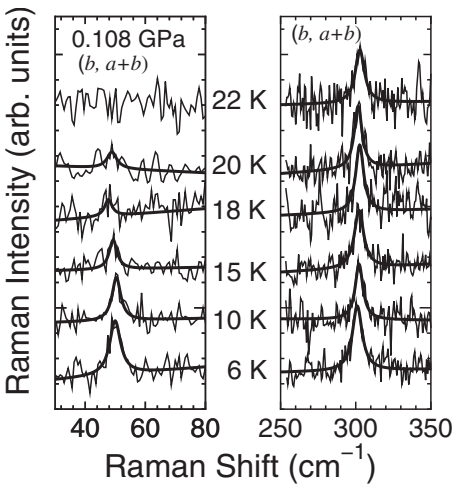

FIG. 3. Temperature dependence of the $(b,b+a)$ Raman spectra from the 64 mode and 305 cm^{-1} phonon at 0.108 GPa. The solid lines denote the fitted curves calculated by Eq. (1).

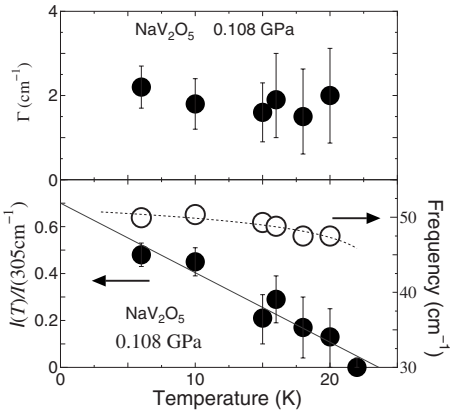

FIG. 4. Temperature dependence of the damping constant Γ, intensity, and frequency of the 64 cm^{-1} mode at 0.108 GPa. The intensity is normalized by the 305 cm^{-1} phonon mode. The solid line denotes a fitted line by the least-square method. The dotted line is only guide for the eye.

Figure 5 shows the T-P phase diagram, which was determined below 2 GPa by means of x-ray diffraction.[23] The dielectric constant was studied under high pressures, suggesting that C_0 phase is stable until 6 GPa.[30] These data above 1 GPa are also plotted but a little bit different from those of x-ray diffraction. The hatched area denotes the complicated superlattice structures with c-axis modulations in the devil's staircase-type phase but the precise feature is omitted here. We plotted T_0, which was obtained from the spin-gap mode, on the T-P phase diagram. The T_0 obtained in the present experiment is in agreement with the critical temperature T_c of x-ray diffraction above 1 GPa, i.e., our result traces the phase boundary between the hatched area and C_0 phase at low pressures and later that between the normal phase P and C_0 phase below about 2 GPa. Here C_0 phase has no modulation along the c axis, i.e., the $(a-b)\times 2b\times 1c$ superlattice structure. However, our result deviates from that of the dielectric constant above 2 GPa and the spin-gap mode could not be detected at 2.71 and 2.74 GPa. We think that it was difficult to detect the spin-gap mode under high pressures, taking into consideration the fact that the anomaly of the dielectric constant at the critical temperature became smaller with increasing pressure in C_0 phase.[30]

It was observed by x-ray diffraction[23] that the superlattice reflections were rather weak and sometimes some of them

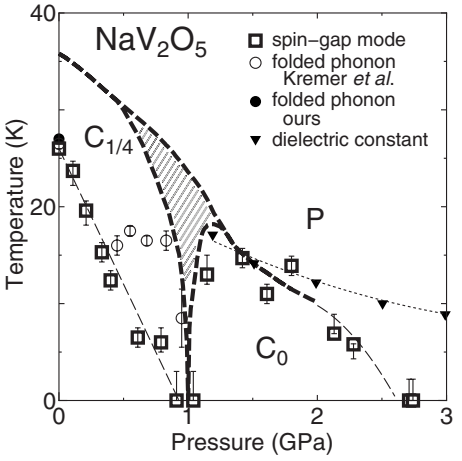

FIG. 5. *T*-*P* phase diagram obtained by Raman scattering (open squares) and that by x-ray (thick broken lines) (Ref. 23). Thin broken lines are only guide for the eye. Open circles show the temperatures where the 944 cm^{-1} folded phonon vanishes, which were reported by Kremer *et al.* (Ref. 24). The result of the dielectric constant (triangles, dotted line) above 1 GPa is also plotted (Ref. 30).

coexisted in the hatched area with complicated superlattice structures, indicating that the long-range order did not grow enough. Then we could not observe the 64 cm^{-1} mode in the complicated superlattice structures.

On the other hand, below 1 GPa, i.e., in $C_{1/4}$ phase, our result deviated largely from T_c of x-ray diffraction. The T_0 obtained by Raman scattering is about 10° lower than T_c by x-ray diffraction. A similar result was obtained for the pressure dependence of the 950 cm^{-1} folded phonon below about 0.5 GPa by Kremer *et al.*,[24] whose result is also plotted in Fig. 5. However, their result is different from that of the 64 cm^{-1} mode above 0.5 GPa. We also measured the temperature dependence of the Raman spectrum of the 646 cm^{-1} folded phonon at 0 GPa in order to confirm T_0, as shown in Fig. 6. It disappeared between 25 and 26 K, which is in good agreement with the result of the 64 cm^{-1} mode and other Raman-scattering results.[15–17,24]

Figure 7 shows a comparison between the low-temperature Raman spectra with $(a,a+b)$ polarization at 1.43 GPa and those with (a,a) and (a,b) polarizations at 0 GPa. In the $(a,a+b)$ polarization, we can observe the folded phonons in $C_{1/4}$ phase.[15] We observed the spin-gap mode at 0 and 1.43 GPa but did not observe the folded phonons at 646 and 944 cm^{-1} when the lattice modulation along the *c* direction does not exist at 1.43 GPa. These folded phonons come from the zone-boundary phonons probably at the Z point (0,0,1/2). The 944 cm^{-1} folded phonon is a pair of the 960 cm^{-1} phonons, reflecting the flat dispersion curves along the *c* direction due to the layered structure in NaV_2O_5. Since C_0 phase has no superlattice modulations along the *c* axis, the 944 cm^{-1} folded phonon was not observed. Similar explanation may be applicable to the 646 cm^{-1} folded phonon.

Figure 8 shows Raman spectrum from the 64 cm^{-1} mode at 0 GPa when a magnetic field of 10 T is applied almost parallel to the *c* axis. The 64 cm^{-1} mode neither shifts in

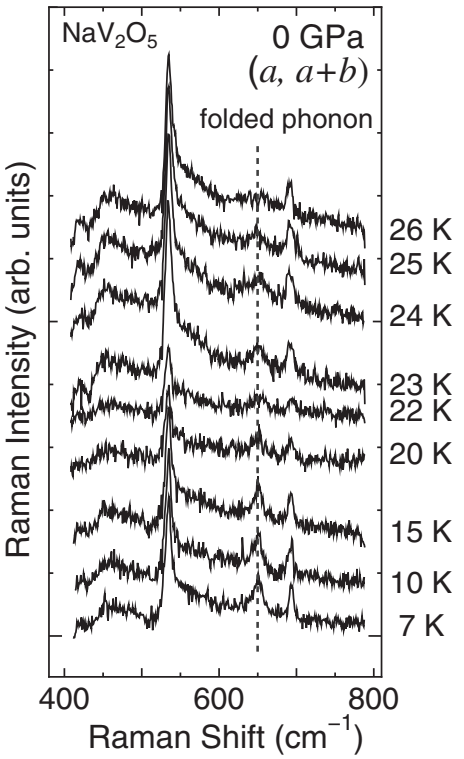

FIG. 6. Temperature dependence of the $(a,b+a)$ Raman spectrum from the 646 cm^{-1} folded phonon at 0 GPa.

frequency nor splits. This result is consistent with those by Fischer *et al.*[17] and by Gozar and Blumberg.[21]

IV. DISCUSSION

We studied Raman scattering in NaV_2O_5 at low temperatures under high pressures. As shown in Fig. 5, below 2 GPa in C_0 phase, the two results by the x-ray diffraction and Raman scattering are in good agreement, but in $C_{1/4}$ phase the T_0 obtained by Raman scattering was about 10° lower than the T_c obtained by x-ray diffraction. Moreover, the tem-

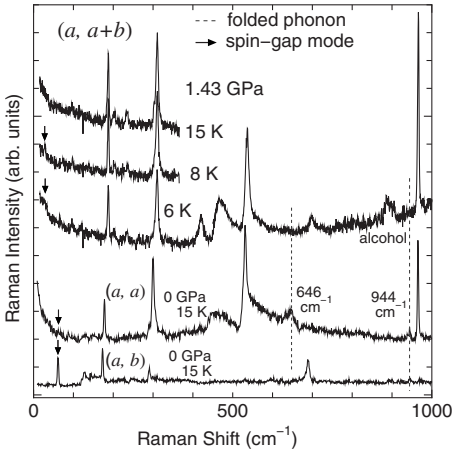

FIG. 7. Comparison between the low-temperature Raman spectra with $(a,a+b)$ polarization at 1.43 GPa and those with (a,a) and (a,b) polarizations at 0 GPa.

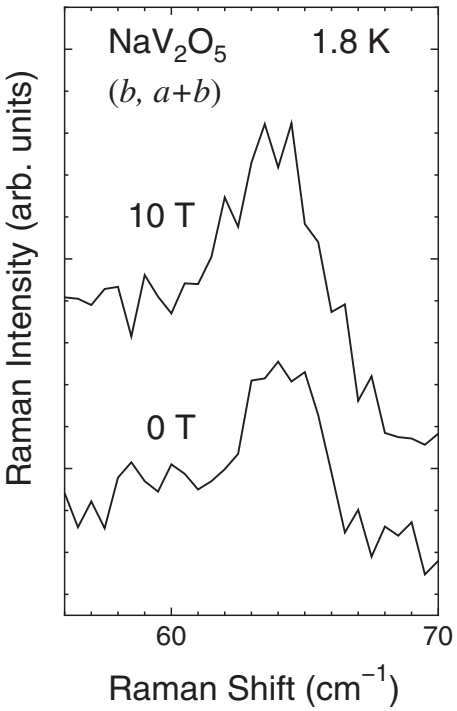

FIG. 8. Raman spectrum from the 64 cm^{-1} mode at 0 GPa and 1.8 K when a magnetic field of 10 T is applied almost parallel to the c axis in addition to that at 0 T.

perature T_0 where the 64 cm^{-1} mode vanished at 0 GPa is in good agreement with the result obtained from the temperature dependence of the folded phonon.

In Raman-scattering measurement, the incident laser often heats the opaque sample. We carefully checked the rise of the sample temperature and estimated that it was within 1°. The charge-order phase-transition temperature T_c decreases drastically with increasing sodium deficiency.[15,20] However, we checked T_c at 0 GPa in our samples by measuring the magnetic susceptibility. Consequently, we think that the deviation of T_0 from T_c in $C_{1/4}$ phase is intrinsic.

The driving force of the phase transition of this compound is considered as Coulomb interactions[2,9] and as a result a zigzag charge ordering is formed. Raman scattering from the magnetic excitations and the folded phonons is, therefore, sensitive to the charge disproportion parameter δ, which will be later discussed in detail.

We focus on the 64 cm^{-1} mode to study the devil's staircase-type phase transition under high pressures. Although the 64 cm^{-1} mode at 0 GPa coincides with the energy E_g^+ of the triplet excitation observed by inelastic neutron scattering, the origin of this mode has been controversial until now.[21] The main points of the controversy is that the 64 cm^{-1} mode does not show the magnetic field dependency, as shown in Fig. 8. Moreover, the first-order Raman scattering from magnetic excitation by the spin-orbit interaction mechanism is forbidden in the spin-gap systems.[28]

The spin system above T_c can be modeled by two-dimensional Hamiltonian in the ab plane

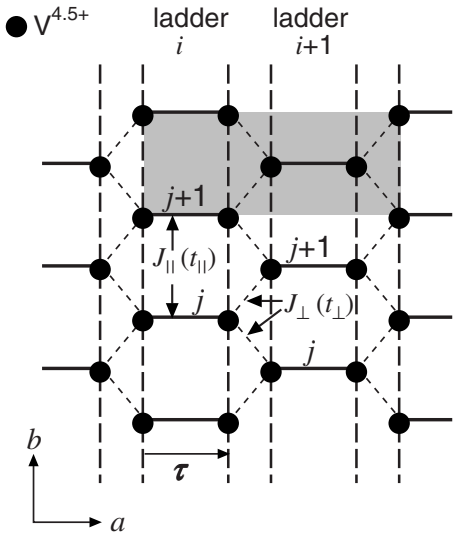

FIG. 9. The spin-ladder structure of V ions on the ab plane of NaV_2O_5 at room temperature. The shadowed area denotes the high-temperature primitive unit cell.

$$\mathcal{H} = J_{\parallel} \sum_{i,j} \boldsymbol{s}_{i,j} \cdot \boldsymbol{s}_{i,j+1} + J_{\perp} \sum_{i,j} (\boldsymbol{s}_{i,j} \cdot \boldsymbol{s}_{i+1,j} + \boldsymbol{s}_{i,j} \cdot \boldsymbol{s}_{i+1,j+1}), \quad (2)$$

where $\boldsymbol{s}_{i,j}$ is a spin on the jth rung in the ith ladder, and $J_{\parallel}$ and $J_{\perp}$ are the exchange interactions between two spins on the adjacent rungs in a ladder and between those in the nearest-neighboring ladders, respectively, as shown in Fig. 9.

The $(a-b)\times 2b\times 4c$ superlattice structure is formed below $T_c=34$ K at ambient pressure. There are four rungs on the ab plane in the low-temperature primitive unit cell, which are labeled as rung $\ell=1-4$, as shown in Fig. 10. Grenier *et al.*[8] studied the magnetic excitations by inelastic neutron scattering and stated that for each ladder the distortions in the exchange paths both within the ladder and via neighboring ladder results in an alternation of the exchange coupling $J_{\parallel}$ in the b direction, $J_{\parallel 1}$ and $J_{\parallel 2}$ $(J_{\parallel 1} > J_{\parallel 2})$, in the charge-ordered state. This alternation of the exchange inter-

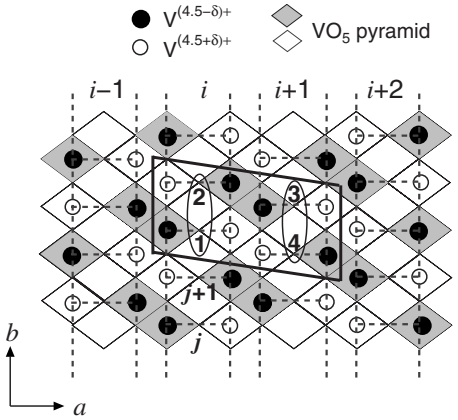

FIG. 10. Zigzag model and monoclinic structure below T_c. The area enclosed by bold lines denotes the low-temperature primitive unit cell. There are four rungs in a unit cell. The ellipses denote the spin-singlet states.

action in a ladder creates the spin-singlet pairs in the neighboring rungs. Two kinds of this ladder are alternatively formed along the a axis, leading to the creation of two branches of the magnetic excitations. This magnetic structure is approximately regarded as a weakly interacting zigzag-chain system.

Although the spin-gap mode is originally Raman inactive in the first-order (one-magnon) Raman scattering, it becomes allowed at the magnetic Γ point when the spin-singlet ground state is mixed with the spin-triplet excited state in the magnon Bose-Einstein condensation phase[27] of $TlCuCl_3$ and the impurity-doped spin-Peierls compound $CuGeO_3$.[28] This idea is also applicable to the present case. Then we may consider only the wave functions on these four rungs in the primitive unit cell.

We should take into consideration that the spin gap opens together with a zigzag charge ordering below T_c. However, the charge order is not perfect so that the charge disproportion parameter δ plays a crucial role in the Raman-scattering process. Damascelli *et al.*[31] consider each rung as an independent linear molecule of two V^{5+} ions and the eigenstates of the additional electron in between are bonding and antibonding wave functions. Smolinski *et al.*[32] studied the band structure in the density-functional calculation and stated that an antiferromagnetic superexchange interaction between the spins on a doubly occupied rung of the ladder is working through the oxygen ions. The electron hopping between the left and right sides on a rung creates the kinetic exchange. Moreover, the ground state is nonmagnetic even in the charge-ordered state. Then we assume that the up-spin and down-spin states are completely mixed in the V-O-V molecular orbitals of $V^{4.5+}$ ions on rung ℓ above T_c and the wave functions of the nth electron in rung ℓ may be written by

$$\chi_\ell^+(n) = \frac{1}{\sqrt{2}}\{|\ell L\uparrow\rangle_n + i|\ell R\downarrow\rangle_n\}, \tag{3}$$

possessing an energy of $-E_0$ and

$$\chi_\ell^-(n) = \frac{1}{\sqrt{2}}\{|\ell L\uparrow\rangle_n - i|\ell R\downarrow\rangle_n\} \tag{4}$$

with an energy of E_0, where $E_0 > 0$.

In the charge-ordered state below T_c, the following additional crystal pseudopotential $V(\boldsymbol{r})$ is formed on a rung by choosing our origin of coordinates halfway between two V ions in a rung,

$$V(\boldsymbol{r}) = V_L\left(\boldsymbol{r} - \frac{\boldsymbol{\tau}}{2}\right) + V_R\left(\boldsymbol{r} + \frac{\boldsymbol{\tau}}{2}\right), \tag{5}$$

where $\boldsymbol{\tau}$ is the vector of rung in a ladder, as shown in Fig. 9. The Hamiltonian is given as

$$\mathcal{H}_{\text{rung}} = \begin{pmatrix} -E_0 + V_S & V_A \\ V_A & E_0 + V_S \end{pmatrix}. \tag{6}$$

Here

$$V_S \simeq \frac{1}{2}\{\langle \ell L|V_L(\boldsymbol{r})|\ell L\rangle + \langle \ell R|V_R(\boldsymbol{r})|\ell R\rangle\}, \tag{7}$$

$$V_A \simeq \frac{1}{2}\{\langle \ell L|V_L(\boldsymbol{r})|\ell L\rangle - \langle \ell R|V_R(\boldsymbol{r})|\ell R\rangle\}. \tag{8}$$

Probably, the additional symmetric pseudopotential V_S is nearly zero in the charge-ordered state and the charge ordering originates from the antisymmetric pseudopotential V_A.[33,34] In rung $\ell = 1$, as shown in Fig. 10, $V_A < 0$ and the following low-energy states with an energy of $-E_{\text{rung}}$ are given as

$$\phi_n(1L\uparrow) = u|1L\uparrow\rangle_n + iv|1R\downarrow\rangle_n. \tag{9}$$

In this state, the electron stays mainly near the left-hand side, i.e., $u > v$. The high-energy states with an energy of $+E_{\text{rung}}$ are given as

$$\phi_n(1R\downarrow) = u|1R\downarrow\rangle_n + iv|1L\uparrow\rangle_n, \tag{10}$$

where the electron favors the right-hand side. Here

$$E_{\text{rung}} = \sqrt{E_0^2 + V_A^2} \tag{11}$$

and $(E_{\text{rung}} - E_0) < |V_A|$. In rung $\ell = 2$, $V_A > 0$ and the low-energy states are given by

$$\phi_n(2R\uparrow) = u|2R\uparrow\rangle_n - iv|2L\downarrow\rangle_n \tag{12}$$

while the high-energy state by

$$\phi_n(2L\downarrow) = u|2L\downarrow\rangle_n - iv|2R\uparrow\rangle_n. \tag{13}$$

Here u and v can be rewritten as by using the charge disproportion parameter δ $(0 \le \delta \le 0.5)$,

$$u = \sqrt{\frac{1+2\delta}{2}}, \tag{14}$$

$$v = \sqrt{\frac{1-2\delta}{2}}. \tag{15}$$

It is noted that $\phi_n(1L\downarrow) = u|1L\downarrow\rangle_n + iv|1R\uparrow\rangle_n$ and $\phi_n(1L\uparrow)$ are degenerate and so on because of the Krammers theorem, when the orbital wave functions are real under the crystal field.

Let us discuss the electronic states for two electrons on rungs $\ell = 1$ and 2 in a ladder, which form the zigzag structure in a ladder, by Hubbard Hamiltonian given as

$$\mathcal{H}_{\text{el}} = -E_{\text{rung}} \sum_{\nu=1L,2R} \sum_{\kappa=\uparrow,\downarrow} c_{\nu\kappa}^\dagger c_{\nu\kappa} - t_\parallel \sum_{\kappa=\uparrow,\downarrow} (c_{1L\kappa}^\dagger c_{2R\kappa} + c_{2R\kappa}^\dagger c_{1L\kappa}) + U(c_{1L\uparrow}^\dagger c_{1L\uparrow} c_{1L\downarrow}^\dagger c_{1L\downarrow} + c_{2R\uparrow}^\dagger c_{2R\uparrow} c_{2R\downarrow}^\dagger c_{2R\downarrow}) \tag{16}$$

because the electron staying at the left-hand side is in the low-energy state in rung 1 and that at the right hand is in the low-energy state in rung 2. Here $\nu = 1L$ and $2R$ means the electronic states of rungs 1 and 2 written by Eqs. (9) and (12), respectively, $c_{\nu\uparrow(\downarrow)}^\dagger$ and $c_{\nu\uparrow(\downarrow)}$ are the creation and annihilation operators of these states with an up (down) spin, respectively, and $-t_\parallel$ (<0) is the hopping energy between two adjacent rungs in a ladder. U is the on-site Coulomb

energy and $E_{\rm rung} > U > 0$. By using the following basis wave functions:

$$\chi_1 = \|\phi(1L\uparrow)\phi(2R\uparrow)\|_-, \quad \chi_2 = \|\phi(1L\uparrow)\phi(2R\downarrow)\|_-,$$

$$\chi_3 = \|\phi(1L\downarrow)\phi(2R\uparrow)\|_-, \quad \chi_4 = \|\phi(1L\downarrow)\phi(2R\downarrow)\|_-,$$

$$\chi_5 = \|\phi(1L\uparrow)\phi(1L\downarrow)\|_-, \quad \chi_6 = \|\phi(2R\uparrow)\phi(2R\downarrow)\|_-, \tag{17}$$

where

$$\|\phi(1L\uparrow)\phi(2R\uparrow)\|_\pm = \frac{1}{\sqrt{2}}\{\phi_1(1L\uparrow)\phi_2(2R\uparrow) \pm \phi_2(1L\uparrow)\phi_1(2R\uparrow)\} \tag{18}$$

and so on, we obtain

$$\mathcal{H}_{\rm el} = \begin{pmatrix} -2E_{\rm rung} & 0 & 0 & 0 & 0 & 0 \\ 0 & -2E_{\rm rung} & 0 & 0 & -t_\parallel & -t_\parallel \\ 0 & 0 & -2E_{\rm rung} & 0 & t_\parallel & t_\parallel \\ 0 & 0 & 0 & -2E_{\rm rung} & 0 & 0 \\ 0 & -t_\parallel & t_\parallel & 0 & -2E_{\rm rung}+U & 0 \\ 0 & -t_\parallel & t_\parallel & 0 & 0 & -2E_{\rm rung}+U \end{pmatrix}. \tag{19}$$

When $t_\parallel \ll U$ we obtain two degenerate excited states, χ_5 and χ_6 with an energy of $(-2E_{\rm rung}+U)$, and the following four states. The charge-ordered spin-singlet state between rungs 1 and 2, whose energy is $(-2E_{\rm rung}-4t_\parallel^2/U)$, is given as

$$\Phi_\sigma(1,2) = \frac{1}{\sqrt{2}}(\chi_2 - \chi_3) = |A_+\rangle_{12}|\sigma\rangle_{12} + i|B_-\rangle_{12}|x\rangle_{12}, \tag{20}$$

where

$$|A_\pm\rangle_{12} = u^2\||1L\rangle|2R\rangle\|_\pm - v^2\||1R\rangle|2L\rangle\|_\pm, \tag{21}$$

$$|B_\pm\rangle_{12} = uv\{\||1R\rangle|2R\rangle\|_\pm + \||1L\rangle|2L\rangle\|_\pm\} \tag{22}$$

for the orbital wave functions and

$$|\sigma\rangle_{12} = \frac{1}{\sqrt{2}}\{|\uparrow\rangle_1|\downarrow\rangle_2 - |\downarrow\rangle_1|\uparrow\rangle_2\}, \tag{23}$$

$$|x\rangle_{12} = \frac{1}{\sqrt{2}}\{|\downarrow\rangle_1|\downarrow\rangle_2 - |\uparrow\rangle_1|\uparrow\rangle_2\} \tag{24}$$

for the spin wave functions. The charge-ordered spin-singlet state includes not only the spin-singlet dimer state $|\sigma\rangle_{12}$ but also the $S_x=0$ spin-triplet dimer state $|x\rangle_{12}$, i.e.,

$$(s_{1x} + s_{2x})|x\rangle_{12} = 0. \tag{25}$$

Meanwhile, the charge-ordered spin-triplet excited states, whose energies are $-2E_{\rm rung}$, are given as

$$\Phi_x(1,2) = \frac{1}{\sqrt{2}}(\chi_1 - \chi_4) = |A_-\rangle_{12}|x\rangle_{12} + i|B_+\rangle_{12}|\sigma\rangle_{12}, \tag{26}$$

$$\Phi_y(1,2) = i\frac{1}{\sqrt{2}}(\chi_1 + \chi_4) = |A'\rangle_{12}|y\rangle_{12} - |B'\rangle_{12}|z\rangle_{12}, \tag{27}$$

and

$$\Phi_z(1,2) = \frac{1}{\sqrt{2}}(\chi_2 + \chi_3) = |A'\rangle_{12}|z\rangle_{12} + |B'\rangle_{12}|y\rangle_{12}, \tag{28}$$

where

$$|A'\rangle_{12} = u^2\||1L\rangle|2R\rangle\|_- + v^2\||1R\rangle|2L\rangle\|_-, \tag{29}$$

$$|B'\rangle_{12} = uv\{\||1R\rangle|2R\rangle\|_- - \||1L\rangle|2L\rangle\|_-\} \tag{30}$$

for the orbital wave functions and

$$|y\rangle_{12} = i\frac{1}{\sqrt{2}}\{|\uparrow\rangle_1|\uparrow\rangle_2 + |\downarrow\rangle_1|\downarrow\rangle_2\}, \tag{31}$$

$$|z\rangle_{12} = \frac{1}{\sqrt{2}}\{|\uparrow\rangle_1|\downarrow\rangle_2 + |\downarrow\rangle_1|\uparrow\rangle_2\} \tag{32}$$

for the spin-triplet dimer state. The charge-ordered spin-triplet state Φ_x contains the spin-singlet dimer state $|\sigma\rangle$ but Φ_y and Φ_z do not contain $|\sigma\rangle$. Of course, the $S_x = \pm 1$ spin-triplet dimer states are written as

$$|S_x = +1\rangle_{12} = \frac{1}{\sqrt{2}}(|y\rangle_{12} + i|z\rangle_{12}) \tag{33}$$

and

$$|S_x = -1\rangle_{12} = \frac{1}{\sqrt{2}}(|y\rangle_{12} - i|z\rangle_{12}). \tag{34}$$

Then the superexchange interaction $J_\parallel$ between the rungs is given as

$$J_{\parallel} = \frac{4t_{\parallel}^2}{U} \tag{35}$$

and the effective spin Hamiltonian can be introduced by Eq. (2), taking the hopping energy $t_{\perp}$ between adjacent ladders into account.

Hereafter, we discuss only the spin states. Then we replace the orbital wave functions $|A_{\pm}\rangle_{\ell\ell'}$, $|B_{\pm}\rangle_{\ell\ell'}$, $|A'\rangle_{\ell\ell'}$, and $|B'\rangle_{\ell\ell'}$ by constant values $A_{\pm}$, $B_{\pm}$, A', and B', respectively, of which magnitudes are given as

$$A_{\pm} = A = u^2 - v^2 = 2\delta, \tag{36}$$

$$B_{\pm} = B = 2uv = (1 - 4\delta^2)^{1/2}, \tag{37}$$

$$A' = u^2 + v^2 = 1, \tag{38}$$

$$B' = 0. \tag{39}$$

Under this assumption the electron spins are not localized at V ions but distributed over the V-O-V molecular orbitals on the rungs of the ladder.[32] When $T > T_c$, i.e., $\delta = 0$, $A = 0$, and $B = 1$. When $\delta = 0.5$, i.e., the complete disproportion, $A = 1$ and $B = 0$. The relation of $A^2 + B^2 = 1$ holds. Grenier *et al.*[8] and Sawa *et al.*[4] estimated δ as about 0.3 from their neutron-scattering and x-ray-diffraction studies at low temperatures. The whole spin wave function of the ground state below T_c can be expressed as a direct product of the charge-ordered spin-singlet states, Ψ_{σ}, in the primitive unit cell,

$$\begin{aligned}\Psi_{\sigma} &= \Phi_{\sigma}(1,2)\Phi_{\sigma}(3,4) \\ &= A^2|\sigma\rangle_{12}|\sigma\rangle_{34} - B^2|x\rangle_{12}|x\rangle_{34} + i\sqrt{2}AB|\varphi_x^+\rangle,\end{aligned} \tag{40}$$

where

$$|\varphi_{\alpha}^{\pm}\rangle = \frac{1}{\sqrt{2}}(|\sigma\rangle_{12}|\alpha\rangle_{34} \pm |\alpha\rangle_{12}|\sigma\rangle_{34}) \tag{41}$$

for $\alpha = x$, y, or z. The $S_x = 0$ charge-ordered spin-triplet states are given as $\Phi_{\sigma}(1,2)\Phi_x(3,4)$ and $\Phi_x(1,2)\Phi_{\sigma}(3,4)$. Taking the exchange interaction $J_{\perp}$ between adjacent ladders into account, they are written as

$$\begin{aligned}\Psi_x^+ &= \frac{1}{\sqrt{2}}\{\Phi_{\sigma}(1,2)\Phi_x(3,4) + \Phi_x(1,2)\Phi_{\sigma}(3,4)\} \\ &= (A^2 - B^2)|\varphi_x^+\rangle + \sqrt{2}iAB(|\sigma\rangle_{12}|\sigma\rangle_{34} + |x\rangle_{12}|x\rangle_{34})\end{aligned} \tag{42}$$

and

$$\Psi_x^- = \frac{1}{\sqrt{2}}\{\Phi_{\sigma}(1,2)\Phi_x(3,4) - \Phi_x(1,2)\Phi_{\sigma}(3,4)\} = |\varphi_x^-\rangle \tag{43}$$

because

$$\begin{aligned}&\langle\Phi_{\sigma}(1,2)\Phi_x(3,4)|\boldsymbol{s}_1\cdot\boldsymbol{s}_3|\Phi_x(1,2)\Phi_{\sigma}(3,4)\rangle \\ &= -\langle\Phi_{\sigma}(1,2)\Phi_x(3,4)|\boldsymbol{s}_1\cdot\boldsymbol{s}_4|\Phi_x(1,2)\Phi_{\sigma}(3,4)\rangle \\ &= -\langle\Phi_{\sigma}(1,2)\Phi_x(3,4)|\boldsymbol{s}_2\cdot\boldsymbol{s}_3|\Phi_x(1,2)\Phi_{\sigma}(3,4)\rangle \\ &= \langle\Phi_{\sigma}(1,2)\Phi_x(3,4)|\boldsymbol{s}_2\cdot\boldsymbol{s}_4|\Phi_x(1,2)\Phi_{\sigma}(3,4)\rangle = \frac{1}{4}.\end{aligned} \tag{44}$$

They can be regarded as a Davydov pair.[21] On the other hand, we obtain

$$\Psi_y^{\pm} = |\varphi_y^{\pm}\rangle, \quad \Psi_z^{\pm} = |\varphi_z^{\pm}\rangle. \tag{45}$$

Now let us consider the origin of the 64 cm^{-1} Raman peak. Fleury and Loudon[35] presented the theory of Raman scattering by one- and two-magnon excitations. The first-order (one-magnon) Raman scattering can be explained by the spin-orbit interaction mechanism involving an electric dipole coupling which proceeds through a spin-orbit coupling in the magnetic ions. This mechanism does not work in the spin-gap state because the total spin is quenched completely in the spin-singlet ground state.[28] In the second-order magnetic Raman process of magnetic materials, the exchange integral works between the pair of magnetic ions. This mechanism plays an essential role in the spin-singlet ground state because the total spin S_{total} and its z component S_{total}^z are conserved in this Raman process.[28] The Raman Hamiltonian in the photon-induced exchange-interaction mechanism is fundamentally given as[28,35–38]

$$\mathcal{H}_{\mathrm{R}} = \sum_{\langle kk'\rangle} F_{k,k'}(\hat{\boldsymbol{E}}_{\mathrm{in}}\cdot\hat{\boldsymbol{r}}_{k,k'})(\hat{\boldsymbol{E}}_{\mathrm{sc}}\cdot\hat{\boldsymbol{r}}_{k,k'})\boldsymbol{s}_k\cdot\boldsymbol{s}_{k'}, \tag{46}$$

where $\hat{\boldsymbol{E}}_{\mathrm{in}}$ and $\hat{\boldsymbol{E}}_{\mathrm{sc}}$ are the unit vectors of the electric fields of the incident and scattered lights, respectively. Here $\hat{\boldsymbol{r}}_{k,k'}$ is a unit vector connecting $\boldsymbol{s}_k$ and $\boldsymbol{s}_{k'}$, and $F_{k,k'}$ is the matrix element for the Raman process accompanied by simultaneous changes in the spin components at kth and k'th spins. Since the exchange interaction along the c axis is very weak, the Raman Hamiltonian in NaV_2O_5 can be written as

$$\begin{aligned}\mathcal{H}_{\mathrm{R}} &= F_{\parallel 1}(\hat{\boldsymbol{E}}_{\mathrm{in}}\cdot\hat{\boldsymbol{b}})(\hat{\boldsymbol{E}}_{\mathrm{sc}}\cdot\hat{\boldsymbol{b}})(\boldsymbol{s}_1\cdot\boldsymbol{s}_2 + \boldsymbol{s}_3\cdot\boldsymbol{s}_4) \\ &\quad + F_{\parallel 2}(\hat{\boldsymbol{E}}_{\mathrm{in}}\cdot\hat{\boldsymbol{b}})(\hat{\boldsymbol{E}}_{\mathrm{sc}}\cdot\hat{\boldsymbol{b}})(\boldsymbol{s}_1\cdot\boldsymbol{s}_2 + \boldsymbol{s}_3\cdot\boldsymbol{s}_4).\end{aligned} \tag{47}$$

Here $F_{\parallel 1}$ and $F_{\parallel 2}$ comes from the intradimer and interdimer exchange interactions, respectively, in a ladder. There are two kinds of ladder in the charge-ordered state.[8] However, we assume that the coefficients $F_{\parallel 1}$ and $F_{\parallel 2}$ for $\boldsymbol{s}_1\cdot\boldsymbol{s}_2$ are the same as that for $\boldsymbol{s}_3\cdot\boldsymbol{s}_4$, although they are slightly different from each other. Moreover, the Raman Hamiltonian by the interladder exchange interaction is omitted because the first-order Raman-scattering probability from the spin-gap mode by it becomes zero using the following matrix elements:

$$\begin{aligned}\langle\Psi_x^+|\boldsymbol{s}_1\cdot\boldsymbol{s}_4|\Psi_{\sigma}\rangle &= \langle\Psi_x^+|\boldsymbol{s}_2\cdot\boldsymbol{s}_3|\Psi_{\sigma}\rangle \\ &= \langle\Psi_x^+|\boldsymbol{s}_1\cdot\boldsymbol{s}_3|\Psi_{\sigma}\rangle \\ &= \langle\Psi_x^+|\boldsymbol{s}_2\cdot\boldsymbol{s}_4|\Psi_{\sigma}\rangle = 0.\end{aligned} \tag{48}$$

Then we obtain the Raman intensity I from the $S_x=0$ charge-ordered spin-triplet state Ψ_x^+ proportional to

$$I_{\eta\mu} = |E_{\rm in}^{\eta}\alpha_{\eta\mu}(\Psi_x^+)E_{\rm sc}^{\mu}|^2 \tag{49}$$

in the first-order scattering process, where the Raman tensors $\alpha_{\eta\mu}(\Psi_x^+)$ for Ψ_x^+ are given as

$$\alpha_{bb}(\Psi_x^+) = F_{\parallel 1}\langle\Psi_x^+|(\boldsymbol{s}_1\cdot\boldsymbol{s}_2+\boldsymbol{s}_3\cdot\boldsymbol{s}_4)|\Psi_\sigma\rangle = i\sqrt{2}F_{\parallel 1}AB \tag{50}$$

by using the matrix elements

$$\langle\Psi_x^+|\boldsymbol{s}_1\cdot\boldsymbol{s}_2|\Psi_\sigma\rangle = \langle\Psi_x^+|\boldsymbol{s}_3\cdot\boldsymbol{s}_4|\Psi_\sigma\rangle = i\frac{1}{\sqrt{2}}AB \tag{51}$$

in a dimer. On the other hand, we obtain that the Raman intensities are zero for the other charge-ordered triplet states Ψ_x^-, $\Psi_y^{\pm}$, and $\Psi_z^{\pm}$. The $S_x=0$ charge-ordered spin-triplet state Ψ_x^+ neither split nor shifted in energy when the magnetic field was applied parallel to the x direction. Therefore, we assign the 64 $\rm cm^{-1}$ peak as it.

The present selection rules indicate that the spin-gap mode is Raman observable in the (bb) polarization. The 64 $\rm cm^{-1}$ peak was observed strongly in the (bb) polarization configuration and also weakly in the (ab) one.[15] In the spin-singlet dimer, the charge is partially distributed at the right side of a rung while it is distributed at the left side of the other rung, as shown in Fig. 10. Consequently, the zigzag spin chains are formed in the charge-ordered state. Then the unit vector $\hat{\boldsymbol{r}}_{1,2}$ ($\hat{\boldsymbol{r}}_{3,4}$) connecting $\boldsymbol{s}_1$ ($\boldsymbol{s}_3$) and $\boldsymbol{s}_2$ ($\boldsymbol{s}_4$) in Eq. (46) cants toward the a axis from the b axis, resulting in appearing of the a component. Therefore The 64 $\rm cm^{-1}$ peak was weakly observed in the (ab) polarization configuration. Moreover, it was also detected in the (aa) polarization configuration under the resonant condition[19,20] because this polarization is the weakest.

Since the Raman intensity from the $S_x=0$ charge-ordered spin-triplet state Ψ_x^+ is proportional to $(AB)^2=4\delta^2(1-4\delta^2)$, it is zero not only when $\delta=0$ but also when $\delta=0.5$ in the complete charge disproportion. It has a maximum at $\delta=1/2\sqrt{2}\sim 0.35$. Ohwada *et al.* studied x-ray diffraction under high pressures in NaV_2O_5. They observed the temperature dependence of the intensities of the superlattice reflections under high pressures, which fit the relation of $I_s\propto[1-(T/T_c)]^{2\beta}$, where $\beta=0.16$ in $C_{1/4}$ phase and $\beta\sim 0.08$ in C_0 phase. Temperature dependence of the charge disproportion parameter δ has not been reported but I_s reflects δ^2. The fact that β in $C_{1/4}$ phase is larger than that in C_0 phase, suggesting that δ in the latter phase grows more rapidly than the former. Probably the formation of the superlattice modulation along the c axis strongly retards the growth of δ. Then it was difficult to detect it just below T_0 in $C_{1/4}$ phase. Moreover, with increasing pressure in $C_{1/4}$ phase, the intensities I_s of the superlattice reflections decrease, which coincides with the fact that the spin-gap mode decreases in intensity on pressure.

However, only the above-mentioned reason cannot sufficiently explain a large deviation of around 10 K between T_0 and T_c in the phase boundary of $C_{1/4}$ phase. It is worthwhile to note that the magnetic Γ points at $\boldsymbol{q}_{m1}=(0,0,0)$ and $\boldsymbol{q}_{m2}=(1/2,1/2,0)$ do not correspond to the lattice-modulation wave vector $\boldsymbol{q}_s=(1/2,1/2,1/4)$ in $C_{1/4}$ phase. Then we infer a following possibility. The Raman intensity from the $S_x=0$ charge-ordered spin-triplet state Ψ_x^+ should be directly coupled to the formation of δ with $\boldsymbol{q}_s$, i.e., $\delta(\boldsymbol{q}_s)$. They can be coupled with each other by replacing $\delta(\boldsymbol{q}_{m1})$ with $\delta(\boldsymbol{q}_s)\delta(-\boldsymbol{q}_s)$, where $\boldsymbol{q}_{m1}=(0,0,0)$. Then the Raman intensity from the spin-gap mode is approximately proportional to $[\delta(\boldsymbol{q}_s)]^2[\delta(-\boldsymbol{q}_s)]^2\propto[1-(T/T_c)]^{4\beta}$ near T_c and grows slowly with decreasing temperature, and the temperatures T_0 that the spin-gap mode vanished are about 10° lower than the x-ray-diffraction result in $C_{1/4}$ phase. On the other hand, the magnetic Γ point, which is probably located at (1/2,1/2,0) although it has not been observed yet in C_0 phase, corresponds to the lattice-modulation wave vector $\boldsymbol{q}_s$. We, therefore, observed the spin-gap mode even just below T_c. However, it was difficult to detect it above 2.7 GPa because δ decreases on pressure. It is inferred from the weakening of the anomaly of the dielectric constant under high pressures.[30]

This explanation can apply to the folded phonon modes at 646 and 944 $\rm cm^{-1}$ in the present study, which lie probably at the Z point, $\boldsymbol{q}=(0,0,1/2)$. This wave vector is $2\times\boldsymbol{q}_s$ in $C_{1/4}$ phase, where $\boldsymbol{q}_s=(1/2,1/2,1/4)$, suggesting that the Raman intensities of the folded phonon modes are proportional to $\{\delta(\boldsymbol{q}_s)\}^4$ and has a similar temperature dependence to the spin-gap mode. It was observed at ambient pressure by Kuroe *et al.*[15] We speculate that the T_0 obtained by the spin-gap mode deviates from that of the folded phonon mode at high pressures in $C_{1/4}$ phase,[24] as shown in Fig. 5, because the appearance of the complicated superlattice structures affects strongly the long-range ordering of the magnetic structure near T_c.

From a point of view of a weakly interacting zigzag-chain system, the second term of Eq. (47) having the coefficient $F_{\parallel 2}$, which works between the adjacent spin-singlet dimer states in a ladder, creates the second-order magnetic Raman scattering,[28] i.e., two magnetic excitations with wave vectors of $\boldsymbol{q}$ and $-\boldsymbol{q}$. It reflects their density of states when the interaction between them is weak.[26,28,39] The peak at 132 $\rm cm^{-1}$ was ascribed to the second-order Raman scattering from magnetic excitations by this mechanism. It has a tail extending to about 410 $\rm cm^{-1}$,[15–20] although we did not observe this tail in the present experiment. The peak at 132 $\rm cm^{-1}$ comes from the large density at the bottom of the dispersion curves of the magnetic excitations.

Next let us discuss the 86 $\rm cm^{-1}$ Raman peak. Gozar and Blumberg[21] studied it by resonant Raman scattering under high magnetic fields. It is very weak and detectable under the resonant condition, and splits into two peaks when magnetic fields are applied parallel to the b and c axes, but it neither shifts nor splits when a magnetic field is parallel to the a axis. Valentí *et al.*[40] theoretically studied Raman scattering in quasi-one-dimensional antiferromagnetic spin chains considering the Dzyaloshinskii-Moriya (DM) interaction. They concluded that a single magnon excitation probed by Raman scattering should show no splitting in external magnetic field parallel to the DM vector $\boldsymbol{D}$ and it should split into two branches for a field perpendicular to the DM vector. The 86 $\rm cm^{-1}$ Raman peak corresponds to this prediction if the DM vector $\boldsymbol{D}$ is parallel to the a direction.[21] Sakai *et al.*[41]

theoretically studied the selection rule of the ESR absorption from the spin gap by taking the DM interaction into account and they concluded from the experimental result[11] that the DM vector is parallel to the a axis in NaV_2O_5. A similar problem for the far-infrared absorption was discussed by Rõõm *et al.*[14]

Recently, Sawa *et al.*[4] studied the detailed crystal structure in the charge-ordered state below T_c and stated that the structure of $C_{1/4}$ phase consists of four inequivalent V sites on the ab plane and the inversion symmetry is broken between the two rungs forming the spin-singlet state. Damascelli *et al.*[31] also stated that a local charge disproportion on each rung of the ladders destroys the inversion symmetry. This suggests that the antisymmetric DM exchange-interaction works between two spins in the charge-ordered spin-singlet state,

$$\mathcal{H}_{\mathrm{DM}} = \boldsymbol{D} \cdot (\boldsymbol{s}_1 \times \boldsymbol{s}_2 - \boldsymbol{s}_3 \times \boldsymbol{s}_4), \tag{52}$$

where $\boldsymbol{D}$ is the DM vector. When $\boldsymbol{D}$ is parallel to the α direction ($\alpha=x$, y, or z), the ground state is changed by the following matrix element:

$$\langle \Psi_\alpha^- | \mathcal{H}_{\mathrm{DM}} | \Psi_\sigma \rangle = i\rho, \tag{53}$$

where

$$\rho = \begin{cases} D(A^2 - B^2)/\sqrt{2} & \text{for } \boldsymbol{D} \parallel \alpha = x \\ DA^2/\sqrt{2} & \text{for } \boldsymbol{D} \parallel \alpha = y,z. \end{cases} \tag{54}$$

And other matrix elements against the ground state Ψ_σ are zero. This result indicates that the DM interaction mixes the charge-ordered spin-singlet ground state Ψ_σ, whose energy is replaced by zero, with the charge-ordered spin-triplet excited state Ψ_α^- ($\alpha=x,y,z$) possessing an energy of ε_-,

$$\Psi_\sigma(g) = \frac{1}{\sqrt{1 + \left(\frac{E_\sigma}{\rho}\right)^2}} \left(\Psi_\sigma + i \frac{E_\sigma}{\rho} \Psi_\alpha^- \right), \tag{55}$$

$$\Psi_\alpha^-(e) = \frac{1}{\sqrt{1 + \left(\frac{E_e^-}{\rho}\right)^2}} \left(\Psi_\sigma + i \frac{E_e^-}{\rho} \Psi_\alpha^- \right), \tag{56}$$

giving a probability of Raman scattering from the magnetic excitations $\Psi_\alpha^-(e)$. Here the energies E_σ of the ground state $\Psi_\sigma(g)$ and E_e^- of the excited state $\Psi_\alpha^-(e)$ are, respectively, given as

$$E_\sigma = \frac{\varepsilon_- - \sqrt{\varepsilon_-^2 + 4\rho^2}}{2},$$

$$E_e^- = \frac{\varepsilon_- + \sqrt{\varepsilon_-^2 + 4\rho^2}}{2}. \tag{57}$$

When $\boldsymbol{D} \parallel \alpha$ ($\alpha=x,y,z$), we obtain

$$\langle \Psi_\alpha^-(e) | (\boldsymbol{s}_1 \cdot \boldsymbol{s}_2 + \boldsymbol{s}_3 \cdot \boldsymbol{s}_4) | \Psi_\sigma(g) \rangle = -\frac{\rho}{\sqrt{\varepsilon_-^2 + 4\rho^2}} (A^2 - B^2). \tag{58}$$

Then the charge-ordered spin-triplet excited states $\Psi_\alpha^-(e)$ ($\alpha=x,y,z$) become Raman active using the Raman Hamiltonian given by Eq. (47).

Gozar and Blumberg[21] studied the resonant Raman scattering of NaV_2O_5 and observed a spin-gap mode at $E_g^- = E_e^- - E_\sigma = 86$ cm^{-1} in the resonant region of the incident light. Moreover, they observed no change in this peak when the magnetic field is applied parallel to the a axis but a double splitting of this peak when the magnetic field is applied parallel to the b or c axis, which indicates that the DM vector $\boldsymbol{D}$ is parallel to the a crystal axis. Here, we always set the applied magnetic field to be parallel to the x direction. The DM vector $\boldsymbol{D}$ is parallel to the x direction, i.e., the magnetic field, when the magnetic field is parallel to the a axis. Then the 86 cm^{-1} Raman peak neither shifts nor splits.[21] On the other hand, the DM vector $\boldsymbol{D}$ is perpendicular to the applied magnetic field, i.e., the x direction, when the magnetic field is parallel to the b or c axis. The 86 cm^{-1} Raman peak splits into two peaks, taking Eqs. (33) and (34) into account.[21] Therefore, the 86 cm^{-1} Raman peak can be assigned as the charge-ordered spin-triplet excited states $\Psi_\alpha^-(e)$ ($\alpha=x,y,z$), which are activated by the DM interaction. Since the DM interaction is probably weak, i.e., $|\boldsymbol{D}| \ll J_\perp, J_\parallel$, this peak whose Raman intensity is proportional to $\boldsymbol{D}^2$ becomes detectable only under the resonant condition. When the DM interaction exists, the Raman Hamiltonian with the same form as Eq. (52) should be taken into consideration.[40] However, the above result does not change, taking Eqs. (53) and (54) into account.

Meanwhile, another charge-ordered spin-triplet excited state Ψ_x^+ with an energy of ε_+ is not affected by the DM interaction and it was observed at $E_g^+ = \varepsilon_+ - E_\sigma = 64$ cm^{-1} in the present experiment at ambient pressure. The ground state $\Psi_\sigma(g)$ includes a small quantity of the triplet states Ψ_α^- because the DM interaction is weak. Then the energy of $\Psi_\sigma(g)$, E_σ, is almost unchanged under magnetic fields. Therefore, the 64 cm^{-1} Raman peak neither shifts nor splits under the applied magnetic fields. Other charge-ordered spin-triplet excited states Ψ_y^+ and Ψ_z^+, of which energies depend on magnetic field, remain Raman inactive.

V. CONCLUSION

In this paper we studied Raman scattering at low temperatures under high pressures in NaV_2O_5. We observed the spin-gap mode, which appears at 64 cm^{-1} at ambient pressure, not only in $C_{1/4}$ phase but also in C_0 phase of the devil's staircase-type phase structure, indicating that C_0 phase is also a spin-gap state. However, we could not detect it above 2.7 GPa. In $C_{1/4}$ phase, the temperatures that the spin-gap mode vanished are about 10° lower than the x-ray-diffraction result. We discussed the selection rule of the spin-gap mode, taking the charge disproportion parameter δ into

consideration. The incomplete charge disproportion in the zigzag-chain structure plays an essential role in its activation in the Raman-scattering process. The charge-ordered $S_x=0$ spin-triplet state Ψ_x^+ mixes with the spin-singlet ground state and becomes observable in the exchange-interaction Raman process. Therefore, it neither shifts nor splits under magnetic fields. We assigned the spin-gap mode observed in the present experiment as this excited state at the magnetic Γ point. This wave vector does not correspond to that of the superlattice in $C_{1/4}$ phase, leading that the spin-gap mode could not be detected in the vicinity of T_c. The DM interaction introduces that another spin-triplet excited state $\Psi_\alpha^-(e)$ $(\alpha=x,y,z)$ is mixed with the ground state. This mode split when a magnetic field is applied perpendicular to the DM vector. The 86 cm^{-1} mode, which was observed by the resonant Raman scattering,[20,21] is assigned as it.

*t-sekine@sophia.ac.jp

[1] M. Isobe and Y. Ueda, J. Phys. Soc. Jpn. **65**, 1178 (1996).
[2] H. Seo and H. Fukuyama, J. Phys. Soc. Jpn. **67**, 2602 (1998).
[3] H. Nakao, K. Ohwada, N. Takesue, Y. Fujii, M. Isobe, Y. Ueda, M. v. Zimmermann, J. P. Hill, D. Gibbs, J. C. Woicik, I. Koyama, and Y. Murakami, Phys. Rev. Lett. **85**, 4349 (2000).
[4] H. Sawa, E. Ninomiya, T. Ohama, H. Nakao, K. Ohwada, Y. Murakami, Y. Fujii, Y. Noda, M. Isobe, and Y. Ueda, J. Phys. Soc. Jpn. **71**, 385 (2002).
[5] Y. Fujii, H. Nakao, T. Yoshihama, M. Nishi, K. Nakajima, K. Kakurai, M. Isobe, Y. Ueda, and H. Sawa, J. Phys. Soc. Jpn. **66**, 326 (1997).
[6] K. Ohwada, Y. Fujii, Y. Katsuki, J. Muraoka, H. Nakao, Y. Murakami, H. Sawa, E. Ninomiya, M. Isobe, and Y. Ueda, Phys. Rev. Lett. **94**, 106401 (2005).
[7] T. Yosihama, M. Nishi, K. Nakajima, K. Kakurai, Y. Fujii, M. Isobe, C. Kagami, and Y. Ueda, J. Phys. Soc. Jpn. **67**, 744 (1998).
[8] B. Grenier, O. Cepas, L. P. Regnault, J. E. Lorenzo, T. Ziman, J. P. Boucher, A. Hiess, T. Chatterji, J. Jegoudez, and A. Revcolevschi, Phys. Rev. Lett. **86**, 5966 (2001).
[9] M. Aichhorn, M. Hohenadler, E. Ya. Sherman, J. Spitaler, C. Ambrosch-Draxl, and H. G. Evertz, Phys. Rev. B **69**, 245108 (2004).
[10] A. N. Vasil'ev, A. I. Smirnov, M. Isobe, and Y. Ueda, Phys. Rev. B **56**, 5065 (1997).
[11] S. Luther, H. Nojiri, M. Motokawa, M. Isobe, and Y. Ueda, J. Phys. Soc. Jpn. **67**, 3715 (1998).
[12] H. Nojiri, S. Luther, M. Motokawa, M. Isobe, and Y. Ueda, J. Phys. Soc. Jpn. **69**, 2291 (2000).
[13] M. N. Popova, A. B. Sushkov, S. A. Klimin, E. P. Chukalina, B. Z. Malkin, M. Isobe, and Y. Ueda, Phys. Rev. B **65**, 144303 (2002).
[14] T. Rõõm, D. Hüvonen, U. Nagel, Y.-J. Wang, and R. K. Kremer, Phys. Rev. B **69**, 144410 (2004).
[15] H. Kuroe, H. Seto, J. Sasaki, T. Sekine, M. Isobe, and Y. Ueda, J. Phys. Soc. Jpn. **67**, 2881 (1998).
[16] P. Lemmens, M. Fischer, G. Els, G. Güntherodt, A. S. Mishchenko, M. Weiden, R. Hauptmann, C. Geibel, and F. Steglich, Phys. Rev. B **58**, 14159 (1998).
[17] M. Fischer, P. Lemmens, G. Els, G. Güntherodt, E. Ya. Sherman, E. Morré, C. Geibel, and F. Steglich, Phys. Rev. B **60**, 7284 (1999).
[18] M. J. Konstantinović, K. Ladavac, A. Belić, Z. V. Popović, A. N. Vasil'ev, M. Isobe, and Y. Ueda, J. Phys.: Condens. Matter **11**, 2103 (1999).
[19] M. J. Konstantinović, Z. V. Popović, T. Ruf, M. Cardona, A. N. Vasil'ev, M. Isobe, and Y. Ueda, Phys. Status Solidi B **215**, 661 (1999).
[20] M. J. Konstantinović, J. C. Irwin, M. Isobe, and Y. Ueda, Phys. Rev. B **65**, 012404 (2001).
[21] A. Gozar and G. Blumberg, in *Frontiers in Magnetic Materials*, edited by A. V. Narlikar (Springer-Verlag, Berlin, 2005), p. 697.
[22] K. Ohwada, H. Nakao, H. Nakatogawa, N. Takesue, Y. Fujii, M. Isobe, Y. Ueda, Y. Wakabayashi, and Y. Murakami, J. Phys. Soc. Jpn. **69**, 639 (2000).
[23] K. Ohwada, Y. Fujii, N. Takesue, M. Isobe, Y. Ueda, H. Nakao, Y. Wakabayashi, Y. Murakami, K. Ito, Y. Amemiya, H. Fujihisa, K. Aoki, T. Shobu, Y. Noda, and N. Ikeda, Phys. Rev. Lett. **87**, 086402 (2001).
[24] R. K. Kremer, I. Loa, F. S. Razavi, and K. Syassen, Solid State Commun. **113**, 217 (2000).
[25] T. Sekine, M. Jouanne, C. Julien, and M. Balkanski, Phys. Rev. B **42**, 8382 (1990).
[26] H. Kuroe, J. Sasaki, T. Sekine, N. Koide, Y. Sasago, K. Uchinokura, and M. Hase, Phys. Rev. B **55**, 409 (1997).
[27] H. Kuroe, K. Kusakabe, A. Oosawa, T. Sekine, F. Yamada, H. Tanaka, and M. Matsumoto, Phys. Rev. B **77**, 134420 (2008).
[28] T. Sekine, T. Kaneko, H. Kuroe, and T. Masuda, Phys. Rev. B **78**, 134409 (2008).
[29] I. Loa, K. Syassen, and R. K. Kremer, Solid State Commun. **112**, 681 (1999).
[30] Y. Sekine, N. Takeshita, N. Môri, M. Isobe, Y. Ueda, M. Kosaka, and Y. Uwatoko, J. Phys. Soc. Jpn. **70**, 3660 (2001).
[31] A. Damascelli, C. Presura, D. van der Marel, J. Jegoudez, and A. Revcolevschi, Phys. Rev. B **61**, 2535 (2000).
[32] H. Smolinski, C. Gros, W. Weber, U. Peuchert, G. Roth, M. Weiden, and C. Geibel, Phys. Rev. Lett. **80**, 5164 (1998).
[33] J. C. Phillips, *Bonds and Bands in Semiconductors* (Academic, New York, London, 1973).
[34] C. Gros and R. Valenti, Phys. Rev. Lett. **82**, 976 (1999).
[35] P. A. Fleury and R. Loudon, Phys. Rev. **166**, 514 (1968).
[36] J. B. Parkinson, J. Phys. C **2**, 2012 (1969).
[37] V. N. Muthukumar, C. Gros, W. Wenzel, R. Valentí, P. Lemmens, B. Eisener, G. Güntherodt, M. Weiden, C. Geibel, and F. Steglich, Phys. Rev. B **54**, R9635 (1996).
[38] C. Gros, W. Wenzel, A. Fledderjohann, P. Lemmens, M. Fischer, G. Güntherodt, M. Weiden, C. Geibel, and F. Steglich, Phys. Rev. B **55**, 15048 (1997).
[39] T. Sekine, H. Kuroe, J. Sasaki, Y. Sasago, N. Koide, K. Uchinokura, and M. Hase, J. Phys. Soc. Jpn. **67**, 1440 (1998).
[40] R. Valentí, C. Gros, and W. Brenig, Phys. Rev. B **62**, 14164 (2000).
[41] T. Sakai, O. Cépas, and T. Ziman, J. Phys. Soc. Jpn. **69**, 3521 (2000).